Instability-induced pattern formation of photoactivated functional polymers

Henning Galinski[a,b,1,2], Antonio Ambrosio[a,c,1,2], Pasqualino Maddalena[c], Iwan Schenker[d], Ralph Spolenak[b], and Federico Capasso[a]

[a]School of Engineering and Applied Science, Harvard University, Cambridge, MA 02138; [c]CNR-Institute for Superconductors, Oxides and Other Innovative Materials and Devices (SPIN) and Dipartimento di Fisica, Università degli Studi di Napoli Federico II, 80126 Naples, Italy; and [b]Laboratory for Nanometallurgy and [d]Nonmetallic Inorganic Materials, ETH Zurich, CH-8093 Zurich, Switzerland

Edited by Hai-Ping Cheng, University of Florida, Gainesville, FL, and accepted by the Editorial Board October 8, 2014 (received for review May 26, 2014)

Since the pioneering work of Turing on the formation principles of animal coat patterns [Turing AM (1952) *Phil Trans R Soc Lond* B 237(641):37–72], such as the stripes of a tiger, great effort has been made to understand and explain various phenomena of self-assembly and pattern formation. Prominent examples are the spontaneous demixing in emulsions, such as mixtures of water and oil [Herzig EM, et al. (2007) *Nat Mater* 6:966–971]; the distribution of matter in the universe [Kibble TWB (1976) *J Phys A: Math Gen* 9(8):1387]; surface reconstruction in ionic crystals [Clark KW, et al. (2012) *Nanotechnol* 23(18):185306]; and the pattern formation caused by phase transitions in metal alloys, polymer mixtures and binary Bose–Einstein condensates [Sabbatini J, et al. (2011) *Phys Rev Lett* 107:230402]. Photoactivated pattern formation in functional polymers has attracted major interest due to its potential applications in molecular electronics and photoresponsive systems. Here we demonstrate that photoactivated pattern formation on azobenzene-containing polymer films can be entirely explained by the physical concept of phase separation. Using experiments and simulations, we show that phase separation is caused by an instability created by the photoactivated transitions between two immiscible states of the polymer. In addition, we have shown in accordance with theory, that polarized light has a striking effect on pattern formation indicated by enhanced phase separation.

pattern formation | phase separation | photoactivated functional polymers | azobenzene | spinodal decomposition

Azobenzenes, which belong to photochromic materials, are switchable two-state systems with distinct optical, electronic, magnetic, and/or electrochemical properties that can be reversibly converted by irradiation. Since the discovery of the unique photochemical properties of azobenzene in 1937 (1), azobenzenes have been mainly used in the chemical industry. Only recently, after studies of the molecular physics of the photoisomerization of azo dyes have revealed that the photoisomerization reaction occurs on the timescale of a few picoseconds (2, 3), azobenzenes came back into focus as potential photoswitchable materials (4, 5). Azobenzenes have been investigated in terms of ultrafast spectroscopy (4, 6, 7), mechanoisomerization (8), the effect of slow photons (9), two-photon absorption (10) and laser-induced periodic surface structuring (11–17). The latter describes the phenomenon of Turing pattern formation on the surface of an azopolymer film upon exposure to UV or visible light. The outstanding feature of this photoactivated pattern formation is its dependence on both the light's intensity and polarization, which allows for the formation of a large variety of Turing patterns, such as hexagonal cells, parallel stripes, or turbulent structures. Several attempts have been made to understand the underlying physics that controls these various forms of pattern formation (18–23), but a sound picture is still lacking.

In this paper, we demonstrate that the photoactivated pattern formation on azopolymer films can be entirely explained by the physical concept of phase separation of two coexistent immiscible phases in the polymer. A phase separation can be briefly characterized as follows: A (meta)stable configuration subjected to an external perturbation (temperature, light) becomes unstable. The unstable system tends to equilibrate by the formation of two immiscible phases. These two phases tend to separate leading to a spatial reorganization of the system.

In the case of azopolymers, the instability is caused by the random optical excitation of the isomers in the polymer film. Excited by a photon of suitable energy ($\lambda = 200$–550 nm), the azobenzene isomer undergoes a structural transition by inversion or rotation (3), called photoisomerization, and relaxes either in the *trans* or *cis* ground state. The symmetry of the system is broken. The principle of the photoisomerization reaction for one azobenzene isomer is illustrated in Fig. 1*A*. The ground-state energy is characterized by an asymmetric double-well potential (Fig. 1*A*), containing a stable *trans*-isomerization state and a metastable *cis* isomerization state that can further relax to the *trans* state by thermal excitation. It is worthwhile remarking that the asymmetric double-well potential exists only in the presence of an external light in the given wavelength range of 200 to 550 nm, corresponding to the absorption spectra of the azopolymer.

The molecular structure between the *trans* and *cis* state changes from a planar to a 3D configuration (Fig. 1*B*). Although this configurational change reduces the distance between the two benzene rings of the azobenzene group from 1.0 to 0.59 nm (1, 9) it leads to a significant increase in the molecular volume. In a macroscopic system with many azobenzene isomers, such as an azopolymer film, this volumetric difference between *trans*- and *cis*-rich domains results in height undulations of the surface and eventually in

Significance

When azobenzene-containing polymer films are exposed to UV or visible light complex Turing patterns form on the polymer's surface. But despite the large number of applications reported, a physical explanation for the pattern formation in this important class of materials and its dependence on both the lights intensity and polarization is still lacking. In this study, we present a general explanation for the pattern formation on these photoactivated azopolymer films. We believe that our findings are an innovative contribution to the field of pattern formation of functional polymers and photoactivated thin film engineering, which have the potential to boost the development of photoresponsive systems, such as molecular electronic devices.

Author contributions: H.G. and A.A. designed and performed the research; A.A. conducted the AFM imaging; A.A. fabricated the samples; H.G. and I.S. designed the simulation model; H.G. and A.A. analyzed the data; H.G., A.A., I.S., R.S., and F.C. wrote the paper; and P.M., R.S., and F.C. provided conceptual advice.

The authors declare no conflict of interest.

This article is a PNAS Direct Submission. H.-P.C. is a guest editor invited by the Editorial Board.

[1]H.G. and A.A. contributed equally to this work.

[2]To whom correspondence may be addressed. Email: hgalinski@seas.harvard.edu or antonio.ambrosio@spin.cnr.it.

This article contains supporting information online at www.pnas.org/lookup/suppl/doi:10.1073/pnas.1409718111/-/DCSupplemental.

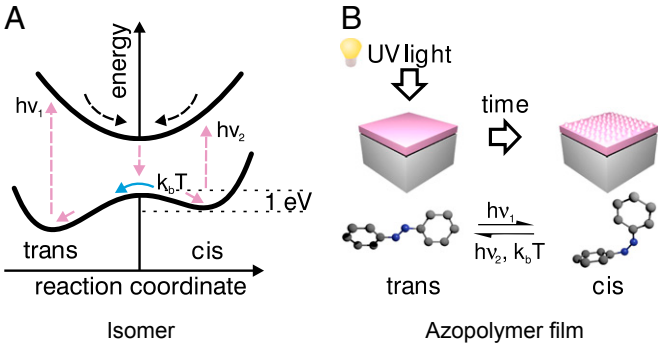

Fig. 1. Effect of photoisomerization on a single azobenzene isomer and an azopolymer film. (*A*) Scheme of the reversible photoisomerization reaction of a single azobenzene isomer. The azobenzene isomer is excited by light $h\nu_i$ (UV/visible range) from the *trans* or *cis* ground state. The isomer falls back to the ground state by inversion or rotation of the molecule and relaxes in either the *trans* or *cis* form by a symmetry-breaking phase transition (pink arrows). The free energy of the ground state is characterized by an asymmetric double-well potential. The energy barrier (1 eV) between the *cis* state and the unstable point allows a direct thermal transition (k_bT) from the *cis* to *trans* state (blue arrow) (52). This means that the *trans*-to-*cis* photoisomerization is merely induced by light $h\nu_1$, whereas the *cis*-to-*trans* photoisomerization can be induced by either light $h\nu_2$ at a smaller photon energy or a thermal transition. (*B*) Schematic description of the light-induced pattern formation on a flat azopolymer film. Exposure to light in the UV/visual range $h\nu_i$ and temperature leads to a random mixture of *cis* and *trans* isomers in the film. The film reduces its free energy by the formation of *trans*- and *cis*-rich microdomains. Because the two isomers have different molecular volumes, an undulation of the surface and the formation of a pattern results.

the formation of patterns (Fig. 1*B*). In other words, the local concentration c of *trans* or *cis* isomers serves as morphological order parameter controlling the undulation of the surface. The tendency to form ordered islands with all molecules in the *trans* state has been experimentally proven by ultrahigh vacuum scanning tunneling microscopy for a monolayer of photochromic molecules on Au(111) (5). Furthermore, the electronic structure of the isomer is altered as the *trans* → *cis* photoisomerization causes an increase of the dipole moment from $p_{\text{trans}} = 0$ Debye to $p_{\text{cis}} = 3$ Debye (6, 24) in combination with an increased electrical resistance of the isomer (4).

In contrast to the photoisomerization of a single isomer that switches its state in the order of a few picoseconds, the formation of the surface pattern in an azopolymer film is significantly slower and in the order of several minutes. The reason for this is a further constriction of the pattern formation in a film by the covalent bonding in the polymer chain and the interaction of each isomer with its immediate environment. Thus, the local free energy f of one *trans* or *cis* isomer in an azopolymer film in the presence of light of a suitable wavelength (λ = 200–550 nm nm) can be expressed as the sum of two contributions: the local free-energy density f_0 of azobenzene isomers covalently bonded to the polymer chain (Fig. 1*A*), and a gradient term $(\nabla c)^2$ that depends on the local concentration. It reads (25)

$$f = f_0 + \frac{\kappa}{2}(\nabla c)^2, \qquad [1]$$

where κ is a positive constant with units of J·m^2 that models the weak short-range interaction. κ is proportional to the width of the transitional regions between the domains (26, 27). As shown by van der Waals in 1893, κ scales inversely with the temperature (28), which in this case is directly proportional to the light intensity. To mimic the landscape of the local free-energy density of the isomers, the Ginzburg–Landau formalism was used such that

$$f_0(c) = -\frac{\epsilon}{2}c^2 + \frac{g}{4}c^4, \qquad [2]$$

where ε and g are positive constants that control the shape of the potential. They depend on the wavelength of the incoming light because the absorption coefficient for *trans* and *cis* isomers varies as a function of the wavelength (29). By integrating Eq. **1**, one obtains an expression for the free energy associated with the short-range interaction F_S in the film in dependence on the free energy

$$F_S(c) = \int \mathrm{d}r\left[-\frac{\epsilon}{2}c^2 + \frac{g}{4}c^4 + \frac{\kappa}{2}(\nabla c)^2\right]. \qquad [3]$$

In contrast to binary alloys or fluids, the photoresponsive monomer cannot move freely in the film as it is covalently bonded to the polymer chain. In other words, the mobility of the azobenzene is constrained by an additional long-range interaction potential, which gives rise to an additional free-energy term F_L. To account for the nonlocal character of this long-range interaction, we have introduced a Green's function $G(r,r')$ that satisfies $\nabla^2 G(r,r') = -\delta(r-r')$ (30). As a result, the long-range interaction term F_L becomes

$$F_L(c) = \frac{B}{2}\int \mathrm{d}r\,\mathrm{d}r' G(r,r')\left[c(r,t)-c_0\right]\left[c(r',t)-c_0\right]. \qquad [4]$$

The parameter c_0 sets the mean volume fraction of *cis* and *trans* isomers and B contributes to the long-range interaction potential in the polymer (31–33).

By superimposing F_S and F_L, one obtains the total free energy F of the film:

$$\begin{aligned} F(c(r,t)) &= F_S(c) + F_L(c) \\ &= \int \mathrm{d}r\left[-\frac{\epsilon}{2}c(r,t)^2 + \frac{g}{4}c(r,t)^4 + \frac{\kappa}{2}|\nabla(c(r,t))|^2\right] \\ &\quad + \frac{B}{2}\int \mathrm{d}r\,\mathrm{d}r' G(r,r')\left[c(r,t)-c_0\right]\left[c(r',t)-c_0\right]. \end{aligned} \qquad [5]$$

Due to the external optical excitation, the local isomer concentration is changing in time, i.e., cis-isomers reversibly switch to *trans* isomers and vice versa. For a given volume, this means that the variation of the free-energy F with respect to the concentration c depends on the local difference of the chemical potentials of *cis* and *trans* isomers (μ_{cis}) and (μ_{trans}), respectively:

$$\frac{\partial F(c)}{\partial c} = (\mu_{\text{cis}} - \mu_{\text{trans}}). \qquad [6]$$

According to Fick's first law, the isomer flux in the system is proportional to the gradient of the chemical potential difference,

$$\boldsymbol{J} = -M\nabla(\mu_{\text{cis}} - \mu_{\text{trans}}). \qquad [7]$$

The parameter M is a phenomenological mobility constant that was set to $M = 1$ (34, 35). As mass conservation is fulfilled in the present case, we can describe the temporal evolution of the local concentration c by using Fick's second law of diffusion, which yields

$$\frac{\partial c}{\partial t} = \Delta(\mu_{\text{cis}} - \mu_{\text{trans}}). \qquad [8]$$

By substituting the chemical potential difference with the variation of the free energy with respect to the concentration (Eq. **6**), one obtains the temporal evolution of the concentration,

$$\frac{\partial c}{\partial t} = \Delta\underbrace{\left(-\epsilon c + gc^3 - \kappa\Delta c\right)}_{F_S} - \overbrace{B(c-c_0)}^{F_L}. \qquad [9]$$

This partial differential equation (PDE) describes how the phase separation alters the local evolution of the isomer concentration, which is directly related to the height undulation on the polymer's surface. The right-hand side of this equation is composed of two terms. As stated above, the first term, F_S, describes the short-range isomer interaction and accounts for the local phase separation due to weak repulsion between *cis* and *trans* isomers. The second term, F_L, describes the long-range interaction in the covalently bonded polymer chain (33). For $B = 0$, Eq. **9** simplifies to the well-known Cahn–Hilliard equation (25). To achieve a computational robust numerical analysis, this PDE was converted into a cell dynamical system (CDS) (36), which satisfies the experimentally observed conditions. A detailed derivation and discussion of the CDS corresponding to this PDE is given in *Materials and Methods*.

Results and Discussion

Unpolarized Light. Experimentally, thin azopolymer films spin-coated on glass were used as the model system. The 700-nm-thick films were exposed to UV light with a wavelength of $\lambda_1 = 337$ nm at normal incidence. At this wavelength the *trans*→ *cis* photoisomerization is most effective (3). The illuminating beam has an elliptical Gaussian profile that results in different illumination doses for different areas of the sample, within the illuminating light spot (*Materials and Methods*). In Fig. 2 the experimentally observed patterns for an irradiated sample are shown and compared with patterns simulated using the CDS model. For both cases, the plots in Fig. 2 show a clear transition from a bicontinuous irregular height pattern (Fig. 2, far left) to a regular height pattern composed of hexagonally packed cylindrical microdomains (Fig. 2, far right). In the experiment, the transition is controlled by an increasing light intensity, whereas in the simulation, the evolution of the pattern is modeled by the coefficient κ. The peaks of the height pattern correspond to *cis*-rich domains and the valleys to *trans*-rich domains. For low intensities (Fig. 2*A*, far left), the height distribution is narrow and a turbulent bicontinuous pattern with a broad interface between *cis*- and *trans*-rich domains is formed. Energetically speaking, the photon density is low and so is the *trans* → *cis* photoisomerization, and the thermally activated *cis* → *trans* back reaction that both control the domain growth. Due to the broad interface between the two domains, one can assume that the formation of the domains is statistically uncorrelated for low intensities.

With increasing intensity, the overall isomerization is enhanced. Locally, this results in the formation of defined domains with a sharp interface. Furthermore, the connectivity of the peaks of the height pattern is partially lost and the *cis*-rich domains undergo locally a continuous–discontinuous transition. At high intensities (Fig. 2*A*, far right), the *cis*-rich domains form a discontinuous array of hexagonally packed cylindrical microdomains. At this stage, the microphase separation saturates and density fluctuations no longer cause severe structural changes. The hexagonal array is characterized by its lattice constant $a = 140$ nm, i.e., the mean distance between the centers of neighboring microdomains, and the mean diameter of these domains $d = 210 \pm 40$ nm. The hexagonal array, as shown in Fig. 2*A* (far right), is distorted by topological defects that arise from the spatially random nucleation of domains. The formation of hexagonal arrays of *cis*-rich domains implies the presence of a long-range interaction between these domains. In the case of diblock copolymer blends, it has been shown that this long-range interaction results from the connectivity of the two different isomers in the polymer chain (30). As this interaction is isotropic, the domains try to maximize the distance between each other, which causes the formation of a

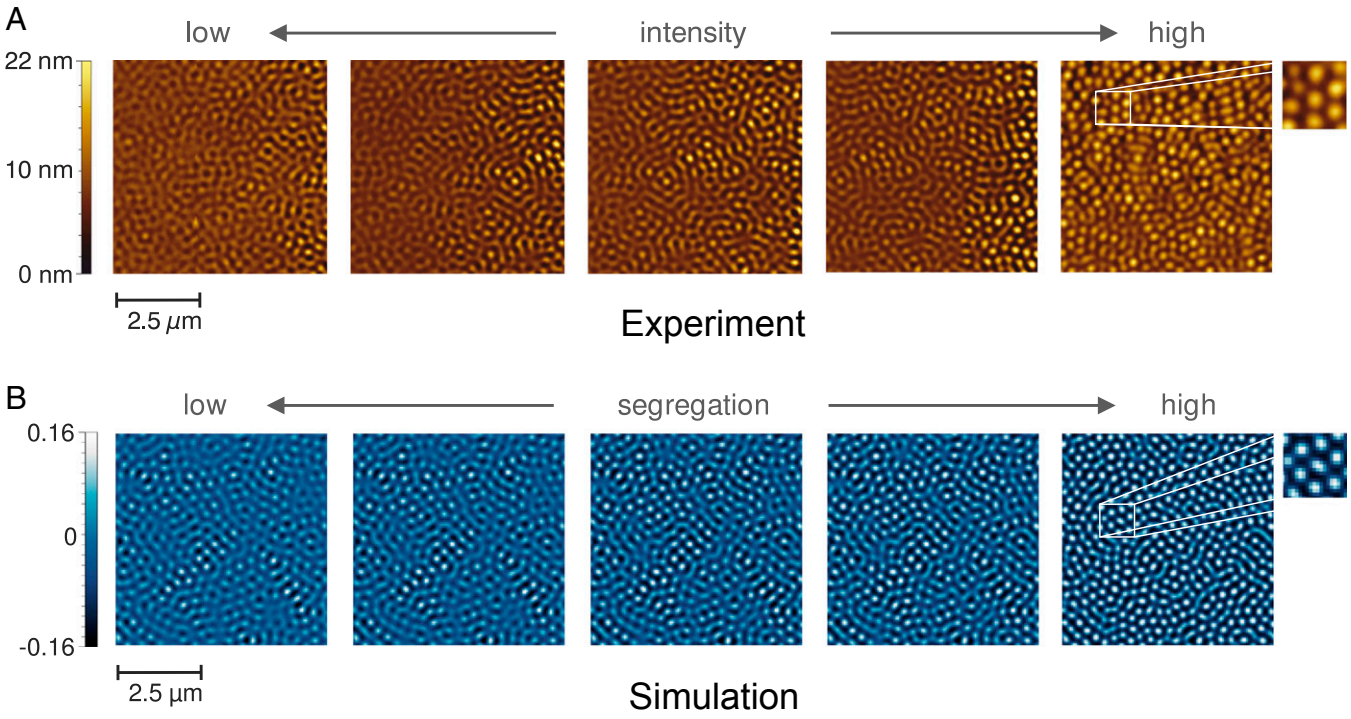

Fig. 2. Experiment and simulation. (*A*) AFM images of different states of pattern formation on the azopolymer films ranging from low intensity (far left) to high intensity (far right) in the illuminating light spot. The colored scale bar indicates the height in nanometers for the first image in each sequence. (*B*) Surface morphologies obtained using the cell dynamics simulation. The colored scale bar indicates the order parameter in arbitrary units. The pattern formation is shown as a function of the coefficient κ that scales inversely with the temperature (28) from 0.39 (far left) to 0.31 (far right). The obtained patterns evolve as a function of the coefficient κ in good agreement with the experimental patterns. The detail in the last image of each sequence illustrates the formation of hexagonal arrays.

hexagonally ordered structure in two dimensions. The formation of equally sized domains (Fig. 2*A*) and a continuous sharpening of interfaces can only occur by diffusion against a concentration gradient and is a key characteristic of spinodal phase separation.

To gain a deeper understanding of the physical mechanisms that control the pattern formation as a function of light intensity, suitable surface descriptors are required that adequately capture the surface evolution and its characteristics. In this paper we have chosen the surface area and the Minkowski functionals (37). In two dimensions, the three Minkowski functionals comprise the covered area m_0; the boundary length m_1; and the Euler number, i.e., the difference between the number of isolated (cylindrical) domains and the number of connected components (valleys) m_2, that relates to the connectivity of the structure. Minkowski functionals are capable of detecting higher orders of spatial correlation and are particularly useful to analyze phase separation phenomena (37). They can be used to test the surface morphology in relationship to its stochastic behavior, e.g., random nucleation (38) (*Materials and Methods*). This further allows the validation of the chosen CDS model. In Fig. 3*A* the surface area evolution as a function of the intensity is depicted and can be well approximated by an exponential dependence. The surface area increases from 25 to 30 μm^2, which corresponds to an increase of 20% in the surface's energy. The experimental result is in good agreement with the simulation. The exponential growth of the surface area can be explained within the context of growing *cis*- and *trans*-rich domains, as the domain growth is the result of the thermally activated shrinking of the mixed regions between the domains (39).

To further substantiate the agreement between experiment and simulation, the experimentally revealed surface morphologies obtained by atomic force microscopy (AFM) are compared with the simulated patterns using Minkowski functionals. In Fig. 3 *B* and *C*, the pattern analysis for the two extrema, i.e., the high and the low intensity case, are shown. In particular, the normalized boundary length m_1 and the normalized Euler number m_2 are plotted as a function of the covered area m_0. The pattern analysis for intermediate intensities is included in *SI Pattern Analysis for Intermediate Light Intensities*. For low intensities, the microdomain formation is locally confined and the domains are randomly distributed on the surface (compare with Fig. 2). The Minkowski functionals in Fig. 3*B* reveal that the overall undulation of the surface evolves consistently with a Gaussian model, depicted as dashed lines. This indicates that for low intensities the domain formation occurs randomly on the surface and the linear dynamics of the microphase separation dominate the pattern formation (40). These characteristics can be attributed to the decelerated photoisomerization reaction, which is due to low photon density and reduced heating of the surface by the laser light.

For high intensities, the behavior of the system is entirely different, which is reflected by a significantly different statistical behavior of the pattern for both the experimental and the simulated data. Fig. 3*C* reveals a deviation from the homogeneous Gaussian behavior seen in Fig. 3*B*, and $m_1(m_0)$ and $m_2(m_0)$ show a pronounced asymmetry. This deviation proves the nonlinear nature of the microphase separation at high intensities, which is substantiated by the saturation of the surface undulation and the formation of defined interfaces on the surface pattern. This is plausible because the repulsion between *cis* and *trans* isomers depends on fluctuations in the local concentration, which are triggered by the intensity-dependent isomerization reaction. In the CDS model the observed nonlinear dynamics is controlled by the ratio between the energy map function and the gradient term, which is controlled by the coefficient κ. In Eq. **9**, this nonlinear dynamics can be identified with the short-range free-energy term F_S.

The structural analysis of the experimentally and computationally obtained patterns has shown that the chosen ansatz of the CDS model quantitatively reproduces the experimental patterns and their statistical signature, such as the transition from linear

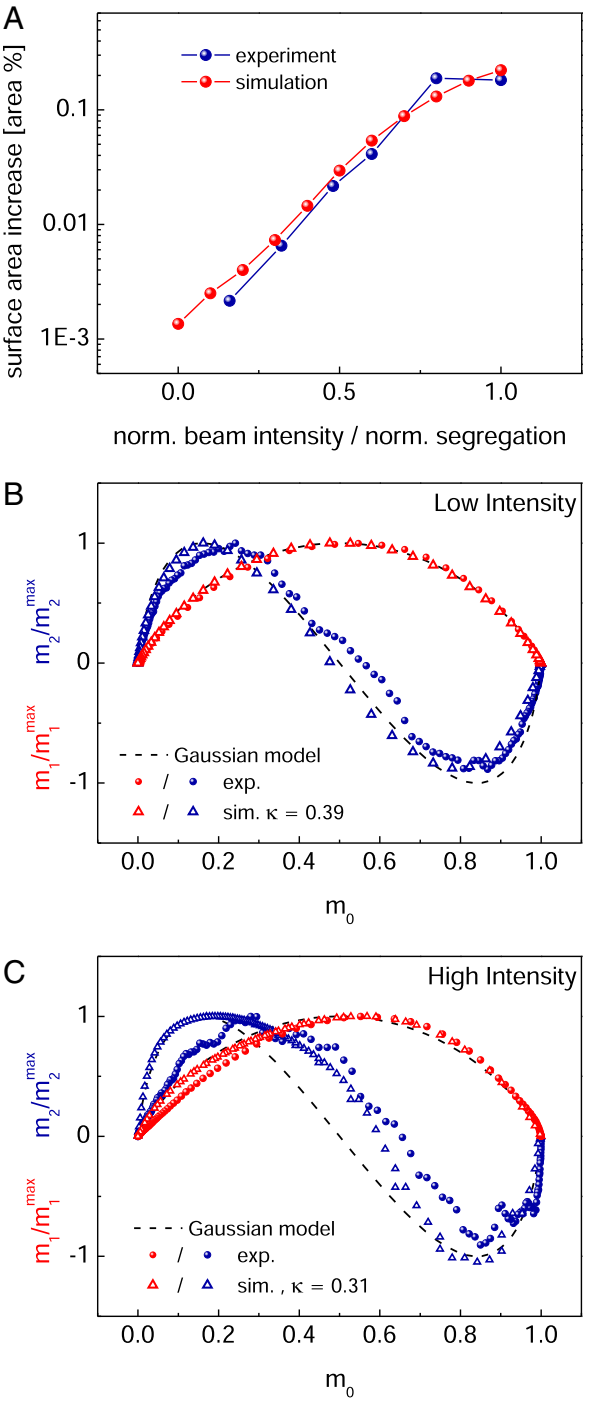

Fig. 3. Pattern analysis. (*A*) The experimentally measured and simulated surface area increases as a function of laser intensity and temperature. The solid lines are a visual to guide the eye. (*B* and *C*) The pattern analysis by Minkowski functionals for the experimental and the simulated azopolymer film patterns for low- and high-intensity state is shown. The normalized boundary length m_1/m_1^{max} and the normalized Euler number m_2/m_2^{max} are plotted as a function of the covered area m_0. All values are normalized to their maximum. The dashed line refers to a surface pattern that evolves like a Gaussian structure. (*B*) For low laser intensities, the experimental and simulated patterns are in good agreement with a Gaussian model. (*C*) For high laser intensities, both the experimental and the simulated patterns show a clear deviation from the Gaussian model (dashed lines). This indicates that the dynamical mechanism that controls the pattern formation is changing as a function of the laser intensity from linear to nonlinear behavior. The deviations between experiment and simulation for small covered areas m_0 are a known experimental artifact that results from the noise floor in the AFM images (53).

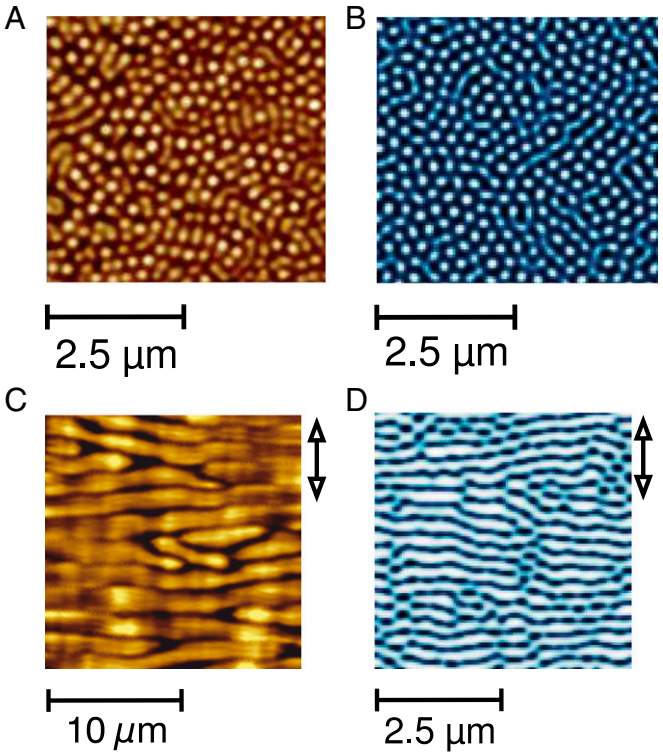

Fig. 4. Pattern formation with polarized and unpolarized light. (*A* and *C*) AFM images of surface patterns formed on azopolymer films by unpolarized (*A*) and linearly polarized (*C*) light. (*B* and *D*) Simulated surface patterns using cell dynamics simulation for unpolarized (*B*) and linearly polarized (*D*) light. In both the experiment and the simulation a clear transition from a cylindrical to stripe pattern is found. The polarization direction is indicated by the black arrow.

to nonlinear dynamics as a function of light intensity. Moreover this model gives a plausible physical explanation of the complex light–matter interaction that controls the pattern formation. It has to be noted that a variation of ε and g instead of κ does not reproduce the experimentally observed statistical features.

Polarized Light. So far the presented results apply only for situations where unpolarized light has been used. Recent results in the literature, however, indicate a direct impact of the polarization on the pattern formation of azopolymers (41). In particular it has been shown that the domain formation is significantly enhanced along the polarization direction. This means that the polarization directly couples to the dipole moment of the azopolymer and creates an additional energy contribution. To account for this experimental fact, we have extended Eq. **9** with a Laplacian $\nabla(\mathbf{n}\cdot\nabla c)$ that describes the direct coupling of the local concentration to the polarization direction of the electric field. The PDE describing the photoactivated phase separation in case of polarized light reads

$$\frac{\partial c}{\partial t} = \alpha\mathbf{n}\cdot\nabla(\mathbf{n}\cdot\nabla c) + \Delta\cdot\left(\frac{\partial F(c)}{\partial c}\right), \qquad [10]$$

where the constant α is proportional to the electric field and $\mathbf{n}$ denotes the polarization direction. Fig. 4 shows AFM images of azopolymer films subjected to unpolarized (Fig. 4*A*) and linearly polarized light (Fig. 4*C*) and the corresponding cell dynamics simulations (Fig. 4 *B* and *D*). The transition from unpolarized to polarized incident light triggers the formation of a lamellar surface pattern instead of a discontinuous array of hexagonally packed cylindrical microdomains. The lamellar pattern is formed perpendicularly to the polarization direction, indicating an enhanced microphase separation of the polymer in the polarization direction. The CDS model qualitatively reproduces the observed experimental pattern and confirms the direct coupling of the polarization to the phase separation of the azopolymer. The difference in feature size of the lamellae can be attributed to the different illumination conditions (*Materials and Methods*) of the azopolymer for the two regimes. The exposure of the azopolymer film to light with a longer wavelength $\lambda = 488$ nm decreases the quantum efficiency of the photoisomerization (3). This decelerates the pattern formation and changes the local concentration of the two isomers in the film. The latter has a direct impact on the pattern formation as it alters the factor $-B(c-c_0)$ in Eq. **9**. It is noteworthy, that this approach is capable of describing the impact of circular or elliptical polarization on the pattern formation, as well.

Conclusion

In this paper we have have presented, for the first time to our knowledge, a general explanation for the photoactivated pattern formation on azopolymer films. This explanation includes patterns formed by polarized and unpolarized light. It has been shown that the photoactivated pattern formation on these films can be explained entirely by the microphase separation of the coexisting *trans* and *cis* isomers in the surface layer of the film. These two isomers are immiscible and products of the *cis* ⇌ *trans* photoisomerization reaction triggered by the external light field. Due to the large variety of surface morphologies that can be created, azopolymers are an ideal model system for the understanding of pattern formation on thin films and, in particular, of their time-dependent kinetics. Here, we were able to reproduce the evolution of the experimentally obtained surface patterns via a cell dynamics simulation using a Cahn–Hilliard model. In agreement with the experimental findings, this model captures the complex kinetics of the pattern formation for different light intensities, including the transition from a linear to a nonlinear regime and the direct coupling of the polarization to the dipole moment of the azopolymer. Beyond the new insight on the underlying physics that control the pattern formation, our work has an immediate impact on the efforts to gain full control over the pattern formation on azopolymer thin films (42, 43) and their application in molecular electronic devices (44–46).

Materials and Methods

Sample Preparation and Characterization. Azopolymer films with a mean thickness of ~700 nm were spin-coated on silica glass substrates. Each (E)-2-(4-((4-methoxyphenyl) diazenyl)phenoxy)ethyl acrylate monomer in the film is composed of an terminal acrylic group and a photoresponsive azobenzene side chain. A detailed description of the material and sample preparation is given in ref. 42. For all experiments conducted with unpolarized light, a nitrogen pulsed laser was used with a nominal energy of 170 μJ per pulse and a wavelength of 337 nm. The pulse width of the laser was less than 3.5 ns, and the repetition rate was 20 Hz. For the experiments where the effect of polarized light on the pattern formation was analyzed, a continuous Ar^+ laser with a nominal wavelength of 488 nm and a beam power of roughly 2 mW was used. Both light sources were focused onto the film using a 75-mm cylindrical lens and in both cases the spot diameter was roughly 120 μm. Due to the different wavelengths and laser energies, different exposure times had to be used. For unpolarized light, the exposure time was set to a few minutes. In the case of polarized light, the samples were exposed for 90 min. We investigated the morphological evolution of the polymer films as a function of the beam intensity through AFM. The related change in surface area and the nanostructures' Minkowski functionals were determined using the Gwyddion software package (gwyddion.net).

Cell Dynamics Simulation. In analogy to pattern formation and phase separation in diblock copolymers (35, 36, 47–49), a conventional CDS model approach was chosen to reproduce the experimentally observed light-induced patterns. The local concentration c is identified with the order parameter ψ of the system $(c=\psi)$. The simulations were performed on a Nvidia GeForce GTX 560 Ti graphics processor unit using Visual C# and

CUDAfy Version 1.22 (cudafy.codeplex.com). The grid had 1,024 × 1,024 positions and periodic boundary conditions (50). For the initial configuration, the order parameter ψ was normally distributed around the mean value $\psi_0 = 0$ with a SD of $\sigma = 0.005$. A constant simulation time of 250 steps was used for all simulations. A detailed description is given in *SI Materials and Methods*.

Structural Analysis via Minkowski Functionals. The experimental data and simulated patterns were analyzed using Minkowski functionals. In two dimensions, the Minkowski functionals m_n are surface descriptors, which capture morphological quantities such as the covered area m_0, the boundary length m_1, the number of isolated (cylindrical) domains, and the number of connected components (valleys), the Euler number m_2. Minkowski functionals are capable of detecting higher orders of spatial correlation and are suited to testing spatial structures for non-Gaussian behavior or features (38, 51). To do so, a given dataset is split into a set of binary data with different threshold levels. In the case of AFM data, the threshold level corresponds to the measured height h. The Minkowski functionals are calculated for each binary dataset and then plotted as a function of the threshold level. This approach allows the investigation of height-specific morphological changes. The experimentally obtained quantities m_n are then tested for non-Gaussian behavior by comparing them with the Minkowski functionals for a Gaussian random field, which are given by

$$m_0(h) = \frac{1}{2}\left(1 - \mathrm{erf}\left(\frac{h}{\sqrt{2}\sigma}\right)\right) \quad [11a]$$

$$m_1(h) = \frac{k}{\sqrt{8\pi}}\exp\left(-\frac{h^2}{2\sigma^2}\right) \quad [11b]$$

$$m_2(h) = \frac{hk^2}{\sqrt{2\pi^3\sigma^2}}\exp\left(\frac{h^2}{2\sigma^2}\right). \quad [11c]$$

σ^2 is the roughness of the film and k corresponds to the second derivative of the covariance in 0. The comparison of spatial surface structures to a Gaussian model is particularly useful, as it allows for the detection of the transition from random uncorrelated to spatially correlated behavior.

ACKNOWLEDGMENTS. H.G. gratefully acknowledges the financial support of the Size Matters! project and A.A. acknowledges funding from the Ministero dell'Istruzione, dell'Università e della Ricerca (Grant PRIN 2010-11-Oxide Interfaces: Emerging New Properties, Multifunctionality, and Devices for Electronics and Energy).

1. Hartley GS (1937) The cis-form of azobenzene. *Nature* 140:281.
2. Yager KG, Barrett CJ (2006) Novel photo-switching using azobenzene functional materials. *J Photochem Photobiol Chem* 182(3):250–261.
3. Fujino T, Arzhantsev SY, Tahara T (2001) Femtosecond time-resolved fluorescence study of photoisomerization of trans-azobenzene. *J Phys Chem A* 105(35):8123–8129.
4. Zhang C, et al. (2004) Coherent electron transport through an azobenzene molecule: A light-driven molecular switch. *Phys Rev Lett* 92(15):158301.
5. Mielke J, et al. (2011) Imine derivatives on Au(111): Evidence for "inverted" thermal isomerization. *ACS Nano* 5(3):2090–2097.
6. Wazzan NA, Richardson PR, Jones AC (2010) Cis-trans isomerisation of azobenzenes studied by laser-coupled NMR spectroscopy and DFT calculations. *Photochem Photobiol Sci* 9(7):968–974.
7. Tait KM, Parkinson JA, Jones AC, Ebenezer WJ, Bates SP (2003) Comparison of experimental and calculated h nmr chemical shifts of geometric photoisomers of azo dyes. *Chem Phys Lett* 374(3-4):372–380.
8. Surampudi SK, Patel HR, Nagarjuna G, Venkataraman D (2013) Mechano-isomerization of azobenzene. *Chem Commun (Camb)* 49(68):7519–7521.
9. Chen JIL, Ozin GA (2008) Tracing the effect of slow photons in photoisomerization of azobenzene. *Adv Mater* 20(24):4784–4788.
10. Ambrosio A, et al. (2009) Two-photon patterning of a polymer containing y-shaped azochromophores. *Appl Phys Lett* 94(1):011115-1–011115-3.
11. Ambrosio A, et al. (2011) Two-photon induced self-structuring of polymeric films based on y-shape azobenzene chromophore. *J Phys Chem C* 115(28):13566–13570.
12. Kulikovska O, Gharagozloo-Hubmann K, Stumpe J, Huey BD, Bliznyuk VN (2012) Formation of surface relief grating in polymers with pendant azobenzene chromophores as studied by AFM/UFM. *Nanotechnology* 23(48):485309.
13. Fang GJ, et al. (2013) Athermal photofluidization of glasses. *Nat Commun* 4:1521.
14. Kang HS, Lee S, Lee SA, Park JK (2013) Multi-level micro/nanotexturing by three-dimensionally controlled photofluidization and its use in plasmonic applications. *Adv Mater* 25(38):5490–5497.
15. Fabbri F, et al. (2012) Kinetics of photoinduced matter transport driven by intensity and polarization in thin films containing azobenzene. *Phys Rev B* 86(11):115440.
16. Patanè S, et al. (2002) Near-field optical writing on azo-polymethacrylate spin-coated films. *Opt Commun* 210(1-2):37–41.
17. Priimagi A, Shevchenko A (2014) Azopolymer-based micro- and nanopatterning for photonic applications. *J Polym Sci, B, Polym Phys* 52(3):163–182.
18. Geue TM, et al. (2002) Formation mechanism and dynamics in polymer surface gratings. *Phys Rev E* 65(5):052801.
19. Yang K, Yang S, Kumar J (2006) Formation mechanism of surface relief structures on amorphous azopolymer films. *Phys Rev B* 73(16):165204.
20. Veer PU, Pietsch U, Saphiannikova M (2009) Time and temperature dependence of surface relief grating formation in polymers containing azobenzene groups with different dipole moment. *J Appl Phys* 106(1):014909.
21. Pedersen T, Johansen P, Holme N, Ramanujam P, Hvilsted S (1998) Mean-field theory of photoinduced formation of surface reliefs in side-chain azobenzene polymers. *Phys Rev Lett* 80(1):89–92.
22. Juan ML, et al. (2009) Multiscale model for photoinduced molecular motion in azo polymers. *ACS Nano* 3(6):1573–1579.
23. Pawlik G, Miniewicz A, Sobolewska A, Mitus AC (2014) Generic stochastic Monte Carlo model of the photoinduced mass transport in azo-polymers and fine structure of surface relief gratings. *EPL* 105(2):26002.
24. Hartley GS, Le Fevre RJW (1939) The dipole moments of cis- and trans-azobenzenes and of some related compounds. *J Chem Soc* 531–535.
25. Cahn JW, Hilliard JE (1958) Free energy of a nonuniform system. I. Interfacial energy. *J Chem Phys* 28(2):258–267.
26. Schmitz G, Ene C, Galinski H, Schlesiger R, Stender P (2010) Nanoanalysis of interfacial chemistry. *JOM* 62(12):58–63.
27. Stender P, Ene CB, Galinski H, Schmitz G (2008) Interface width of immiscible layered elements. *IJMR* 99(5):480–486.
28. Waals J (1979) The thermodynamic theory of capillarity under the hypothesis of a continuous variation of density. *J Stat Phys* 20(2):200–244.
29. Tamai N, Miyasaka H (2000) Ultrafast dynamics of photochromic systems. *Chem Rev* 100(5):1875–1890.
30. Ohta T, Kawasaki K (1986) Equilibrium morphology of block copolymer melts. *Macromolecules* 19(10):2621–2632.
31. Choksi R, Maras M, Williams J (2011) 2D phase diagram for minimizers of a Cahn–Hilliard functional with long-range interactions. *SIAM J Appl Dyn Syst* 10(4):1344–1362.
32. Wu XF, Dzenis YA (2006) Guided self-assembly of diblock copolymer thin films on chemically patterned substrates. *J Chem Phys* 125(17):174707.
33. Bahiana M, Oono Y (1990) Cell dynamical system approach to block copolymers. *Phys Rev A* 41(12):6763–6771.
34. Ren SR, Hamley IW (2001) Cell dynamics simulations of microphase separation in block copolymers. *Macromolecules* 34(1):116–126.
35. Pinna M, Zvelindovsky A (2012) Large scale simulation of block copolymers with cell dynamics. *Eur Phys J B* 85(6):1–18.
36. Oono Y, Puri S (1987) Computationally efficient modeling of ordering of quenched phases. *Phys Rev Lett* 58(8):836–839.
37. Mecke K (2000) *Statistical Physics and Spatial Statistics*, eds Mecke K, Stoyan D, Lecture Notes in Physics (Springer, Berlin), Vol 554, pp 111–184.
38. Mantz H, Jacobs K, Mecke K (2008) Utilizing Minkowski functionals for image analysis: A marching square algorithm. *J Stat Mech-Theory E* 2008(12):P12015.
39. Fratzl P, Lebowitz JL, Penrose O, Amar J (1991) Scaling functions, self-similarity, and the morphology of phase-separating systems. *Phys Rev B Condens Matter* 44(10):4794–4811.
40. Villain-Guillot S, Josserand C (2002) Non-linear dynamics of spinodal decomposition. *Eur Phys J B* 29(2):305–309.
41. Ambrosio A, Girardo S, Camposeo A, Pisignano D, Maddalena P (2013) Controlling spontaneous surface structuring of azobenzene-containing polymers for large-scale nano-lithography of functional substrates. *Appl Phys Lett* 102(9):093102.
42. Ambrosio A, Marrucci L, Borbone F, Roviello A, Maddalena P (2012) Light-induced spiral mass transport in azo-polymer films under vortex-beam illumination. *Nat Commun* 3:989.
43. Ambrosio A, Maddalena P, Marrucci L (2013) Molecular model for light-driven spiral mass transport in azopolymer films. *Phys Rev Lett* 110(14):146102.
44. Henzl J, Morgenstern K (2010) An electron induced two-dimensional switch made of azobenzene derivatives anchored in supramolecular assemblies. *Phys Chem Chem Phys* 12(23):6035–6044.
45. Morgenstern K (2011) Switching individual molecules by light and electrons: From isomerisation to chirality flip. *Prog Surf Sci* 86(5-8):115–161.
46. Liu W, Filimonov SN, Carrasco J, Tkatchenko A (2013) Molecular switches from benzene derivatives adsorbed on metal surfaces. *Nat Commun* 4:2569.
47. Oono Y, Puri S (1988) Study of phase-separation dynamics by use of cell dynamical systems. I. Modeling. *Phys Rev A* 38(1):434–453.
48. Puri S, Oono Y (1988) Study of phase-separation dynamics by use of cell dynamical systems. II. Two-dimensional demonstrations. *Phys Rev A* 38(3):1542–1565.
49. Shiwa Y, Oono Y (1987) Computationally efficient modeling of block copolymer and benard pattern formations. *Mod Phys Lett B* 01(01n02):49–55.
50. Galinski H, et al. (2013) Time-dependent analysis of agglomerating Pt thin films on YSZ single crystals. *C R Phys* 14(7):590–600.
51. Becker J, et al. (2003) Complex dewetting scenarios captured by thin-film models. *Nat Mater* 2(1):59–63.
52. Leyssner F, et al. (2010) Photoisomerization ability of molecular switches adsorbed on Au(111): Comparison between azobenzene and stilbene derivatives. *J Phys Chem C* 114(2):1231–1239.
53. Schmähling J, Hamprecht F (2007) Generalizing the abbott-firestone curve by two new surface descriptors. *Wear* 262(11-12):1360–1371.